Optimisation of a P3 phase with superior high voltage reversibility

Stephanie F. Linnell,[+a, b] Yong-Seok Choi,[+c] Yingling Liao,[a,b] Ioanna M. Pateli,[a, b] Aaron B. Naden,[a] John T. S. Irvine,[a, b] Robert A. House,[b, d] David O. Scanlon,[b,e] A. Robert Armstrong*[, a, b]

[a]School of Chemistry, University of St Andrews, St Andrews, Fife, KY16 9ST, United Kingdom

[b]The Faraday Institution, Quad One, Harwell Science and Innovation Campus, Didcot, OX11 0RA, United Kingdom

[c]Department of Materials and Engineering, Dankook University, 119 Dandae-ro, Cheonan 31116, South Korea

[d]Department of Materials, University of Oxford, Parks Road, Oxford, UK

[e]School of Chemistry, University of Birmingham, Edgbaston, Birmingham B15 2TT, U.K

[+]joint first author

Corresponding Author

*Email: ara@st-andrews.ac.uk

Table S1. *Rietveld refinement results of as-synthesised (a) $Na_{0.7}Mn_{0.75}Ni_{0.25}O_2$, (b) $Na_{0.7}Mn_{0.65}Ni_{0.25}Ti_{0.1}O_2$, (c) $Na_{0.7}Mn_{0.65}Ni_{0.25}Zn_{0.1}O_2$, and (d) $Na_{0.7}Mn_{0.58}Ni_{0.25}Zn_{0.07}Ti_{0.1}O_2$.*

(a) P3 $Na_{0.7}Mn_{0.75}Ni_{0.25}O_2$

R_{wp} : 8.32%, GOF : 1.47

Lattice parameters P3 Space group *R*3*m* *a* = 2.87824(12) Å, *c* = 16.8056(7) Å

Atom	Wyckoff symbol	x/a	y/b	z/c	Occupancy	Uiso×100/ Å^2
Mn1/Ni1	3*a*	0	0	0	0.75/0.25	0.19(6)
Na1	3*a*	0	0	0.1656(9)	0.625(14)	4.7(4)
O1	3*a*	0	0	0.394(2)	1	0.58(11)
O2	3*a*	0	0	0.604(2)	1	0.58(11)

(b) P3 $Na_{0.7}Mn_{0.65}Ni_{0.25}Ti_{0.1}O_2$

R_{wp} : 10.43%, GOF : 1.89

Lattice parameters P3 Space group *R*3*m* *a* = 2.88316(18) Å, *c* = 16.7742(11) Å

Atom	Wyckoff symbol	*x/a*	*y/b*	*z/c*	Occupancy	Uiso×100/ Å^2
Mn1/Ni1/Ti1	3*a*	0	0	0	0.65/0.25/0.1	0.24(7)
Na1	3*a*	0	0	0.16589(11)	0.63(2)	5.7(6)
O1	3*a*	0	0	0.3923(14)	1	0.5
O2	3*a*	0	0	0.6020(15)	1	0.5

(c) P3 $Na_{0.7}Mn_{0.65}Ni_{0.25}Zn_{0.1}O_2$

R_{wp} : 11.35%, GOF : 2.09

Lattice parameters P3 Space group *R*3*m* *a* =2.89046(16) Å, *c* = 16.7638(9) Å

Atom	Wyckoff symbol	*x/a*	*y/b*	*z/c*	Occupancy	Uiso×100/ Å^2
Mn1/Ni1/Zn1	3*a*	0	0	0	0.65/0.25/0.1	0.33(7)
Na1	3*a*	0	0	0.1668(9)	0.64(2)	4.6(5)
O1	3*a*	0	0	0.392(2)	1	0.62(13)
O2	3*a*	0	0	0.6001(2)	1	0.6(13)

(d) P3 $Na_{0.7}Mn_{0.58}Ni_{0.25}Zn_{0.07}Ti_{0.1}O_2$

R_{wp} : 10.32%, GOF : 1.92

Lattice parameters P3 Space group *R*3*m* *a* =2.8953(2) Å, *c* = 16.7843(11) Å

Atom	Wyckoff symbol	*x/a*	*y/b*	*z/c*	Occupancy	Uiso×100/ Å^2
Mn1/Ni1/Zn1/Ti1	3*a*	0	0	0	0.58/0.25/0.07/0.1	0.28(5)
Na1	3*a*	0	0	0.1707(5)	0.633(9)	4.7(4)
O1	3*a*	0	0	0.3921(11)	1	0.62(11)
O2	3*a*	0	0	0.6027(11)	1	0.62(11)

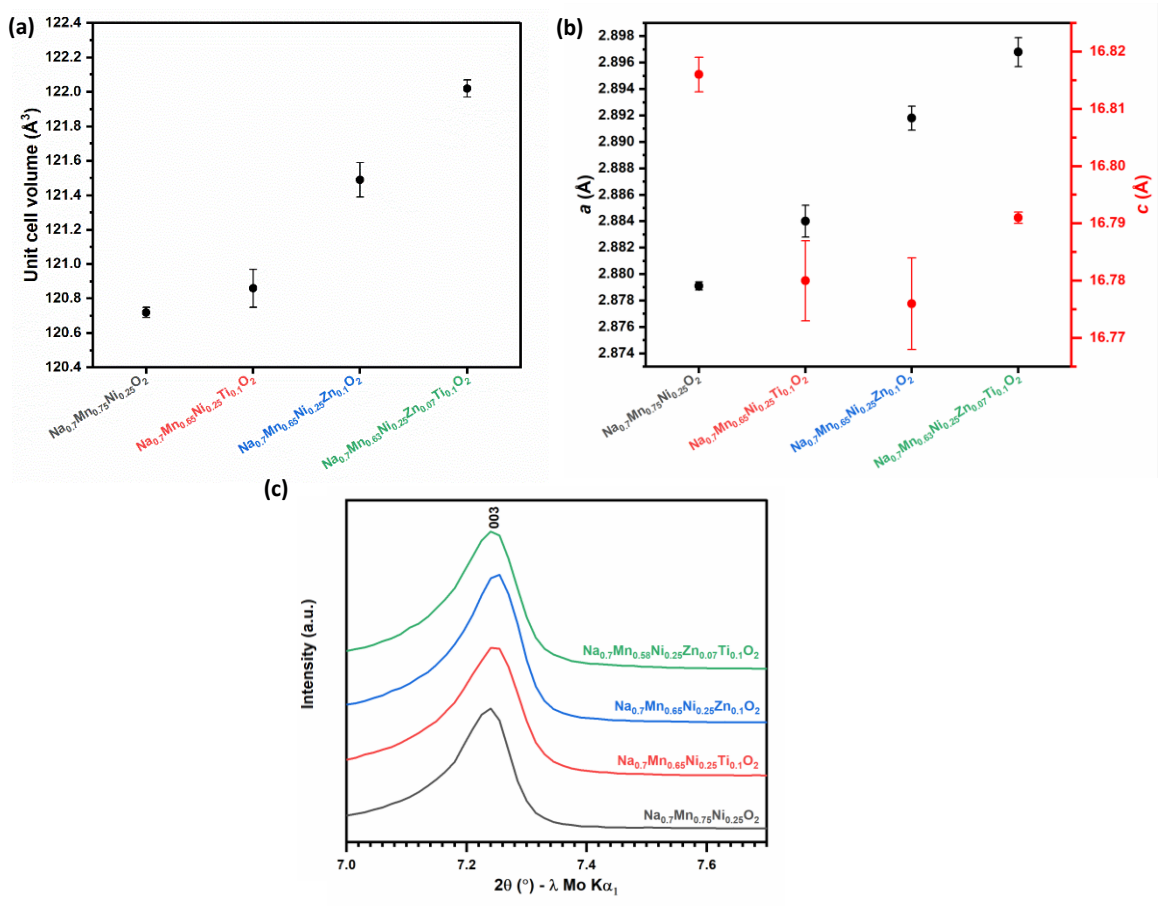

Figure S1. *Comparison between as synthesised* $Na_{0.7}Mn_{0.75}Ni_{0.25}O_2$ *(black),* $Na_{0.7}Mn_{0.65}Ni_{0.25}Ti_{0.1}O_2$ *(red),* $Na_{0.7}Mn_{0.65}Ni_{0.25}Zn_{0.1}O_2$ *(blue) and* $Na_{0.7}Mn_{0.58}Ni_{0.25}Zn_{0.07}Ti_{0.1}O_2$ *(green), as a function of (a) unit cell volume and (b) the a and c unit cell parameters. (c) Laboratory PXRD patterns of as synthesised* $Na_{0.7}Mn_{0.75}Ni_{0.25}O_2$ *(black),* $Na_{0.7}Mn_{0.65}Ni_{0.25}Ti_{0.1}O_2$ *(red),* $Na_{0.7}Mn_{0.65}Ni_{0.25}Zn_{0.1}O_2$ *(blue),* $Na_{0.7}Mn_{0.55}Ni_{0.25}Zn_{0.07}Ti_{0.1}O_2$ *(green) showing the shift of the (003) peak.*

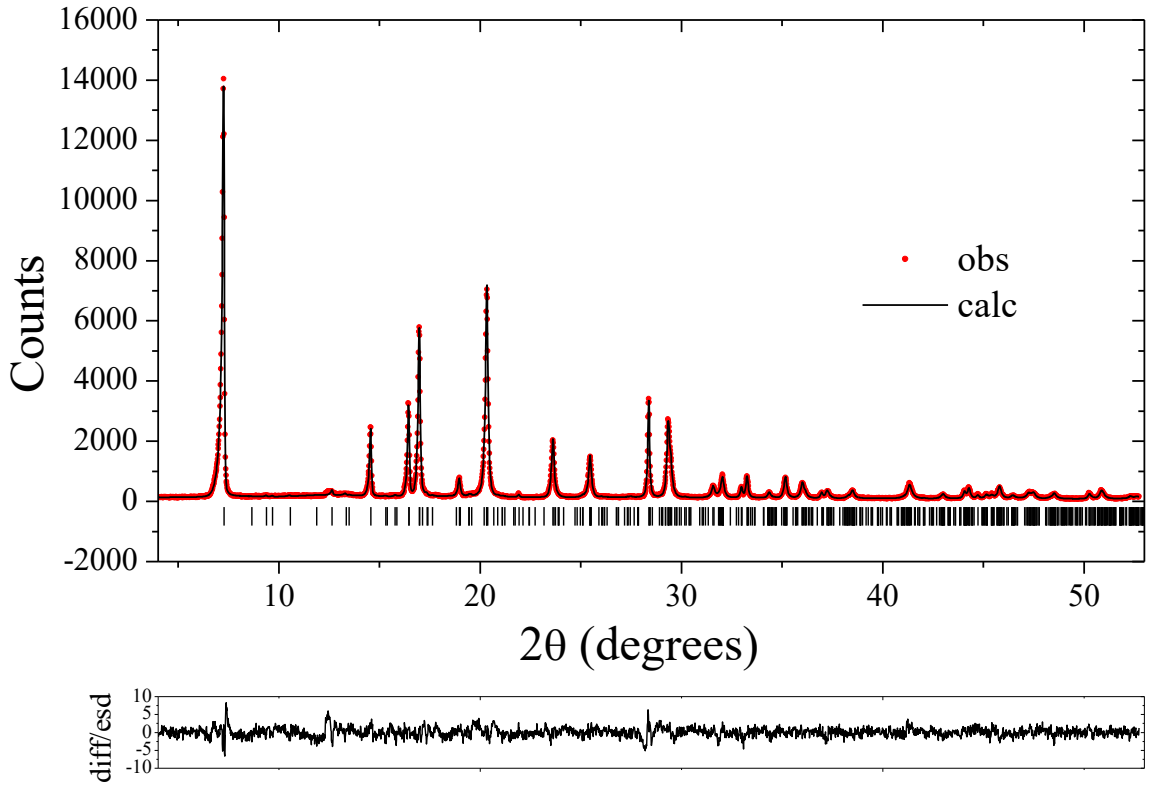

***Figure S2**. Laboratory X-ray Rietveld fit of as-synthesised $Na_{0.7}Mn_{0.65}Ni_{0.25}Zn_{0.1}O_2$, in space group $P2_1/c$. Observed data points are shown in red, with fitted profile in black. Tick marks indicate allowed reflections for the P3 phase.*

***Table S2.** Rietveld refinement results for as-synthesised P3 $Na_{0.7}Mn_{0.65}Ni_{0.25}Zn_{0.1}O_2$ using a superlattice model (space group $P2_1/c$)).*

R_{exp} = 5.40%, R_{wp} = 7.10 %, R_p = 5.09%

Lattice parameters P3 Space Group $P2_1/c$

a = 5.8319(7) Å, b = 8.6774(16) Å, c = 5.0099(7) Å, β = 106.492(6), V = 243.10(7) Å^3

Atom	Wyckoff symbol	x/a	y/b	z/c	Occupancy	Biso
Ni1/Mn1/Zn1	2c	0	0	0.5	0.44(5)/0.40(5)/0.16	0.37(11)
Mn2/Ni2/Zn2	4e	-0.0020(9)	0.3330(7)	0.5019(6)	0.73(5)/0.20(5)/0.07	0.37(11)
Na1	4e	0.4883(17)	0.630(3)	0.289(2)	0.596(13)	1.3(2)
Na2	4e	0.5	0.0	0.371(3)	0.404	1.3(2)
O1	4e	0.824(3)	0.496(3)	0.596(2)	1	0.49(15)
O2	4e	0.182(3)	0.325(3)	0.878(2)	1	0.49(15)
O3	4e	0.800(2)	0.177(3)	0.600(2)	1	0.49(15)

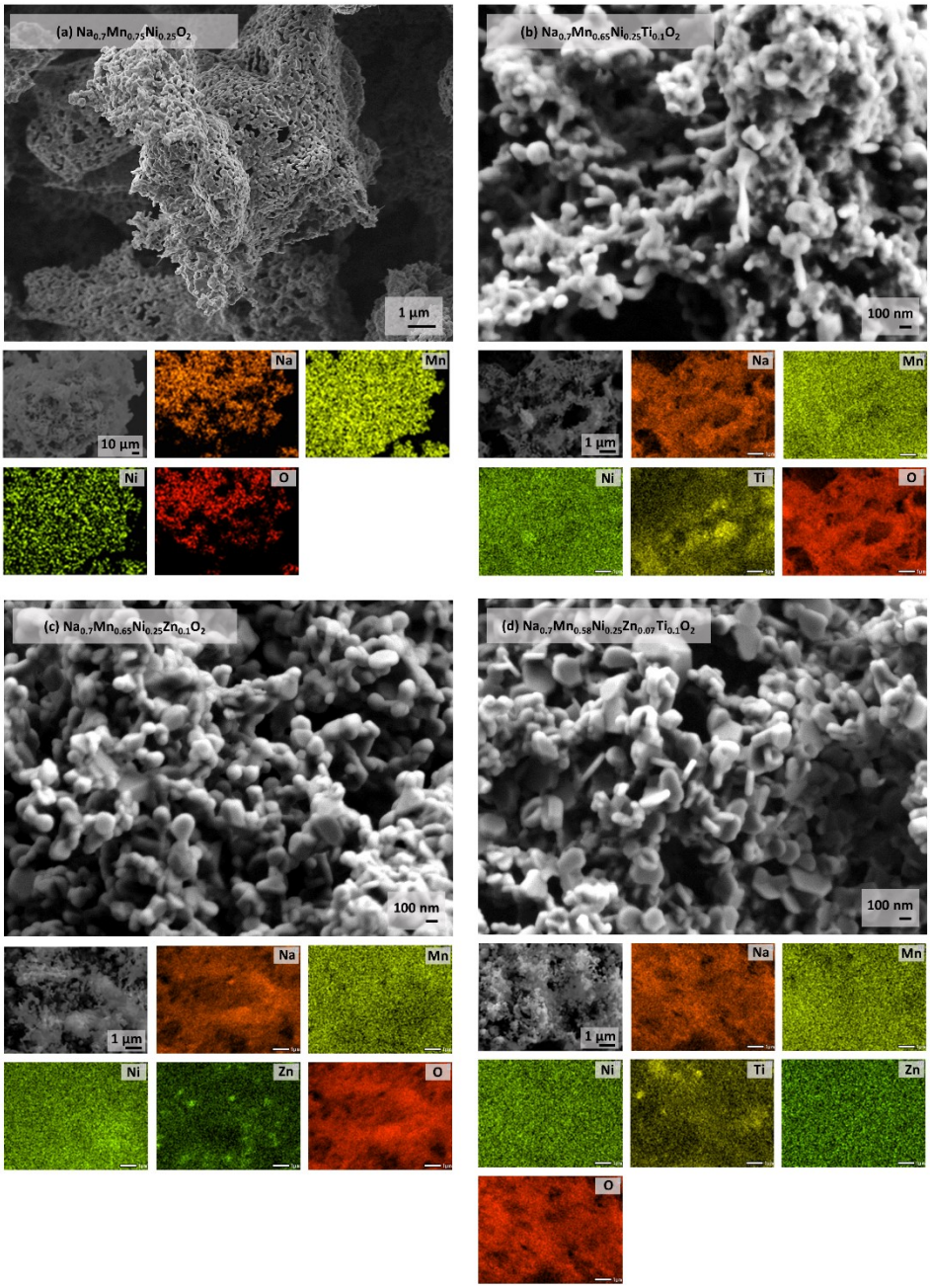

Figure S3. *SEM micrographs (top) and EDS mapping (bottom) of as synthesised (a) $Na_{0.7}Mn_{0.75}Ni_{0.25}O_2$, (b) $Na_{0.7}Mn_{0.65}Ni_{0.25}Ti_{0.1}O_2$, (c) $Na_{0.7}Mn_{0.65}Ni_{0.25}Zn_{0.1}O_2$ and (d) $Na_{0.7}Mn_{0.58}Ni_{0.25}Zn_{0.07}Ti_{0.1}O_2$.*

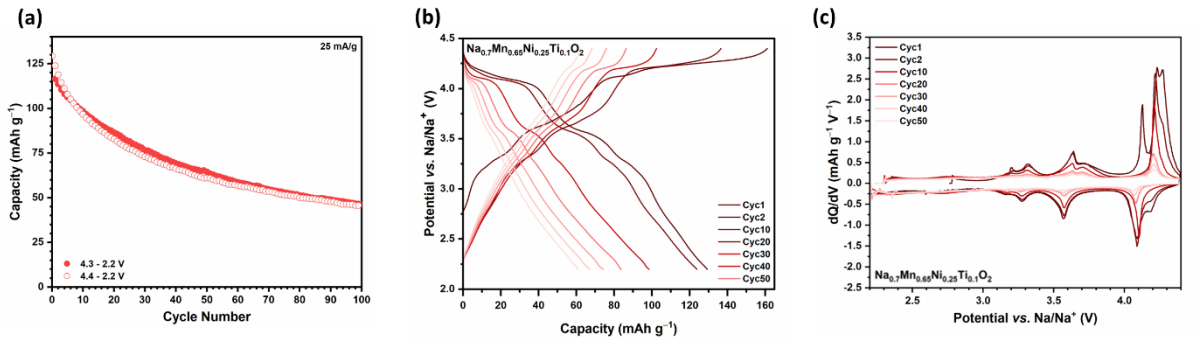

Figure S4. *(a) Galvanostatic cycling performance of half--cells of $Na_{0.7}Mn_{0.65}Ni_{0.25}Ti_{0.1}O_2$ cycled versus Na^+/Na between 2.2--4.3 V (filled spheres) and 4.4--2.2 V (empty sphered) at a rate of 25 mA g^{-1} at 30 °C, showing the discharge capacities. (b) Galvanostatic charge/discharge curves and (c) corresponding differential capacity versus voltage plots of $Na_{0.7}Mn_{0.65}Ni_{0.25}Ti_{0.1}O_2$ cycled versus Na^+/Na at 30 °C between 2.24.4 V at a rate of 25 -mA g^{-1}.*

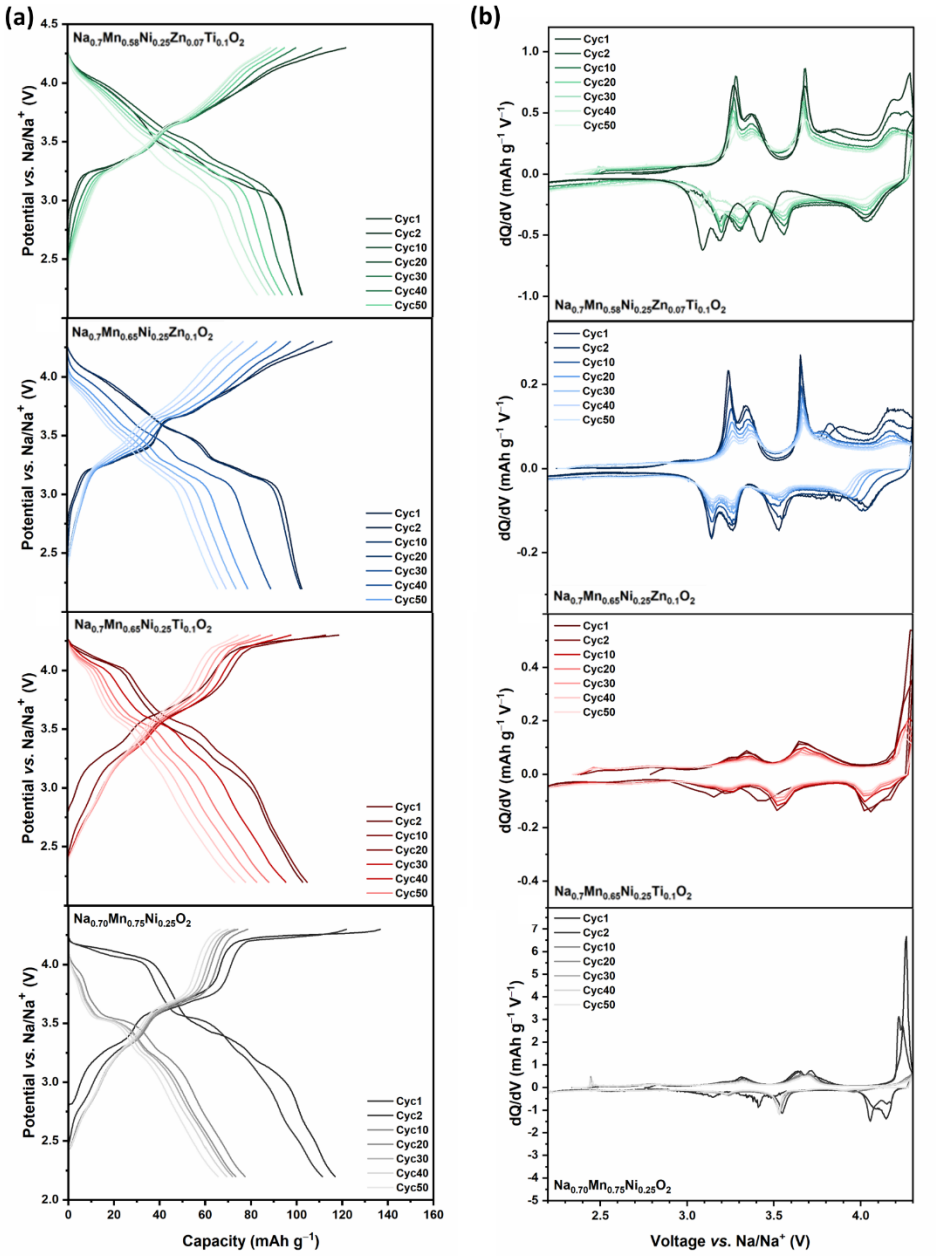

Figure S5. *(a) Galvanostatic charge/discharge curves and (b) corresponding differential capacity versus voltage plots of* $Na_{0.7}Mn_{0.75}Ni_{0.25}O_2$ *(black),* $Na_{0.7}Mn_{0.65}Ni_{0.25}Ti_{0.1}O_2$ *(red),* $Na_{0.7}Mn_{0.65}Ni_{0.25}Zn_{0.1}O_2$ *(blue) and* $Na_{0.7}Mn_{0.58}Ni_{0.25}Zn_{0.07}Ti_{0.1}O_2$ *(green) half--cells cycled versus* Na^+/Na *at 30 °C between 2.2--4.3 V at a rate of 250 mA* g^{-1-}.

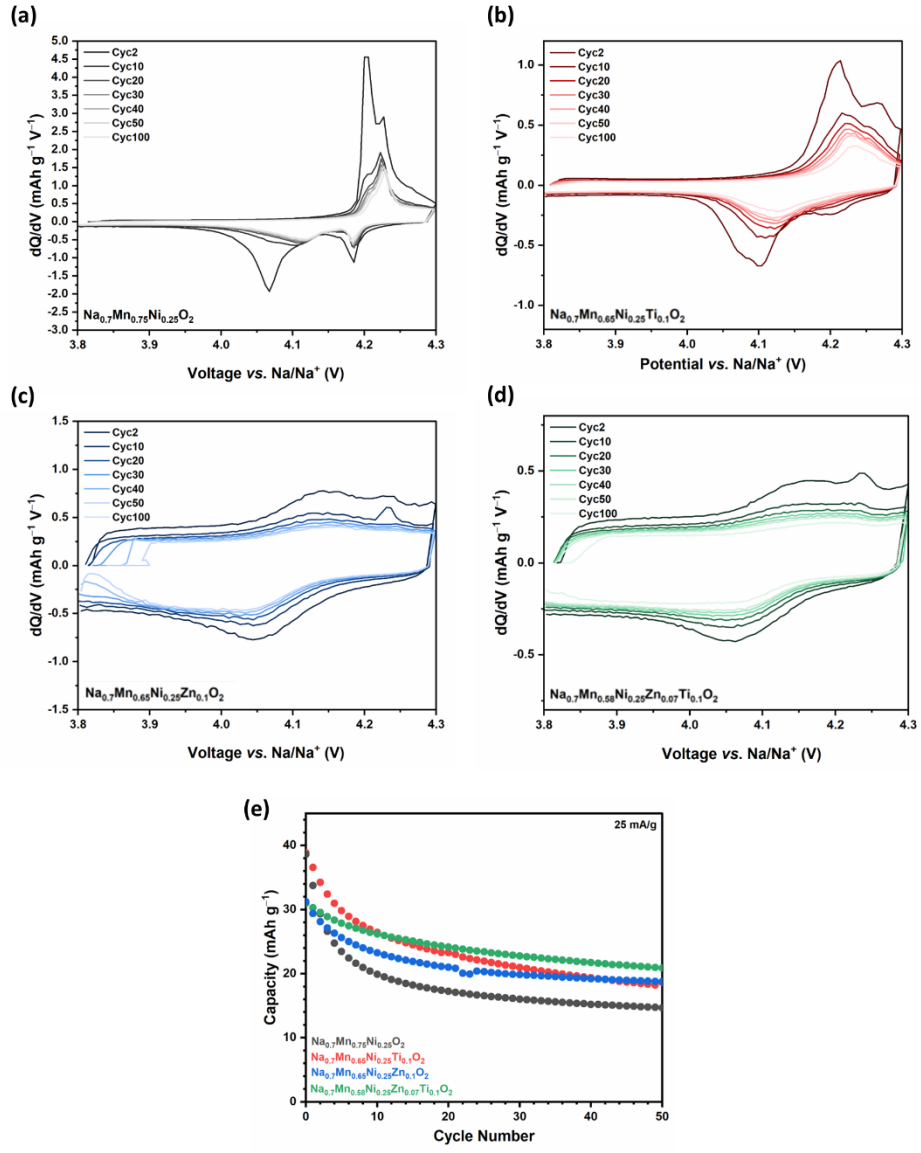

Figure S6. *Differential capacity versus voltage plots of (a) $Na_{0.7}Mn_{0.75}Ni_{0.25}O_2$, (b) $Na_{0.7}Mn_{0.65}Ni_{0.25}Ti_{0.1}O_2$, (c) $Na_{0.7}Mn_{0.65}Ni_{0.25}Zn_{0.1}O_2$ and (d) $Na_{0.7}Mn_{0.58}Ni_{0.25}Zn_{0.07}Ti_{0.1}O_2$ sodium half--cells cycled between 3.8-4.3 V at a rate of 25 mA g^{-1} at 30 °C. (e) Galvanostatic cycling performance of sodium half--cells of $Na_{0.7}Mn_{0.75}Ni_{0.25}O_2$ (black), $Na_{0.7}Mn_{0.65}Ni_{0.25}Ti_{0.1}O_2$ (red), $Na_{0.7}Mn_{0.65}Ni_{0.25}Zn_{0.1}O_2$ (blue) and $Na_{0.7}Mn_{0.58}Ni_{0.25}Zn_{0.07}Ti_{0.1}O_2$ (green) cycled between 3.8--4.3 V at a rate of 25 mA g^{-1} at 30 °C, showing the discharge capacities.*

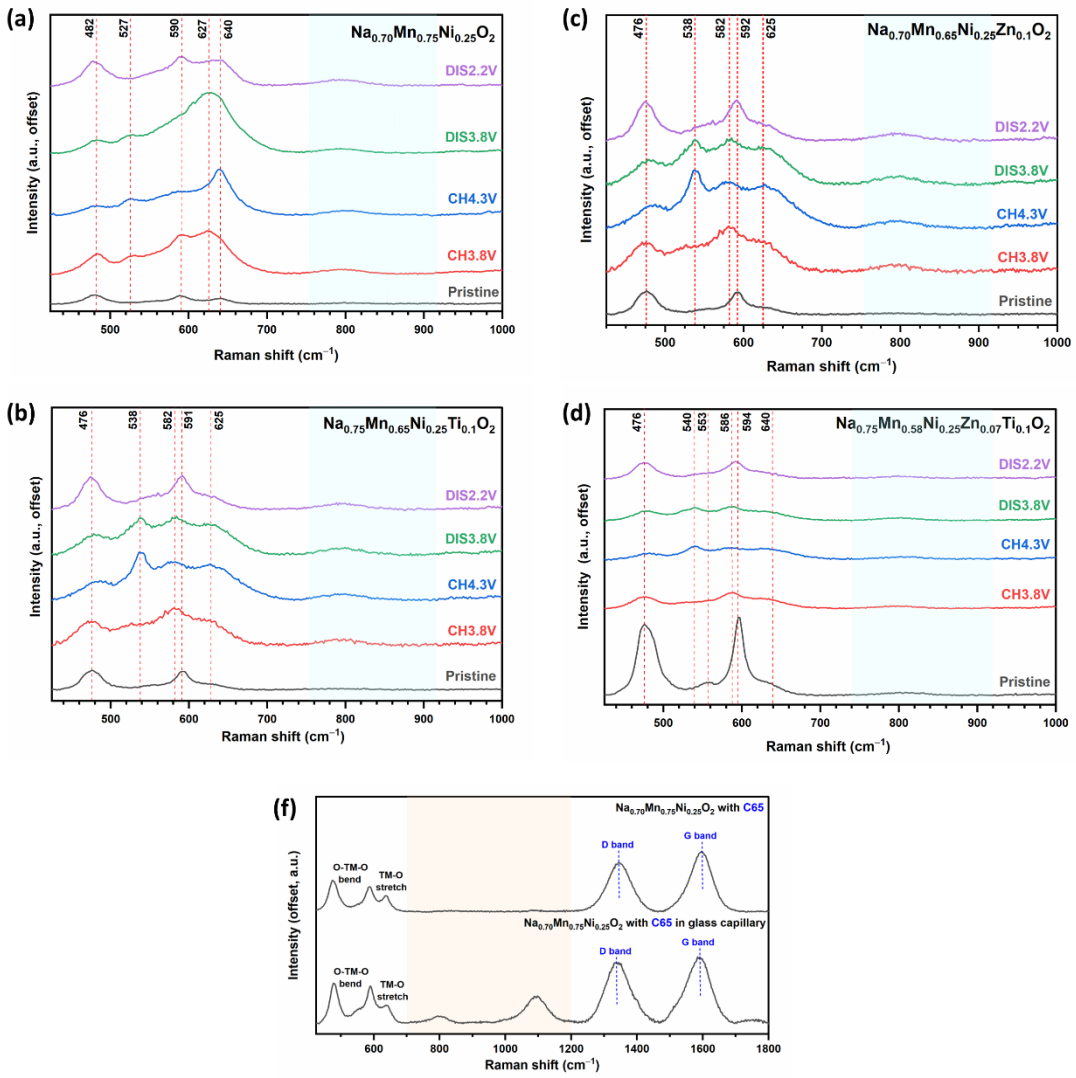

Figure S7. *Ex -situ Raman spectra of (a) $Na_{0.70}Mn_{0.75}Ni_{0.25}O_2$, (b) $Na_{0.75}Mn_{0.65}Ni_{0.25}Ti_{0.1}O_2$, (c) $Na_{0.70}Mn_{0.65}Ni_{0.25}Zn_{0.1}O_2$ and (d) $Na_{0.75}Mn_{0.58}Ni_{0.25}Zn_{0.07}Ti_{0.1}O_2$ electrodes, showing the pristine material (black line), after charge to 3.8 V (red line), charge to 4.3 V (blue line), discharge to 3.8 V (green line) and discharge to 2.2 V (purple line), collected in glass capillaries. (f) Raman spectra of as -synthesised $Na_{0.70}Mn_{0.75}Ni_{0.25}O_2$ mixed with C65 showing bands at ~1346 and ~1598 cm^{-1} attributed to the D and G bands. Raman spectra were collected in (lower) and out (upper) of a glass capillary and the orange region highlights contributions at approximately 800 and 1100 cm^{-1} from the glass capillary.*

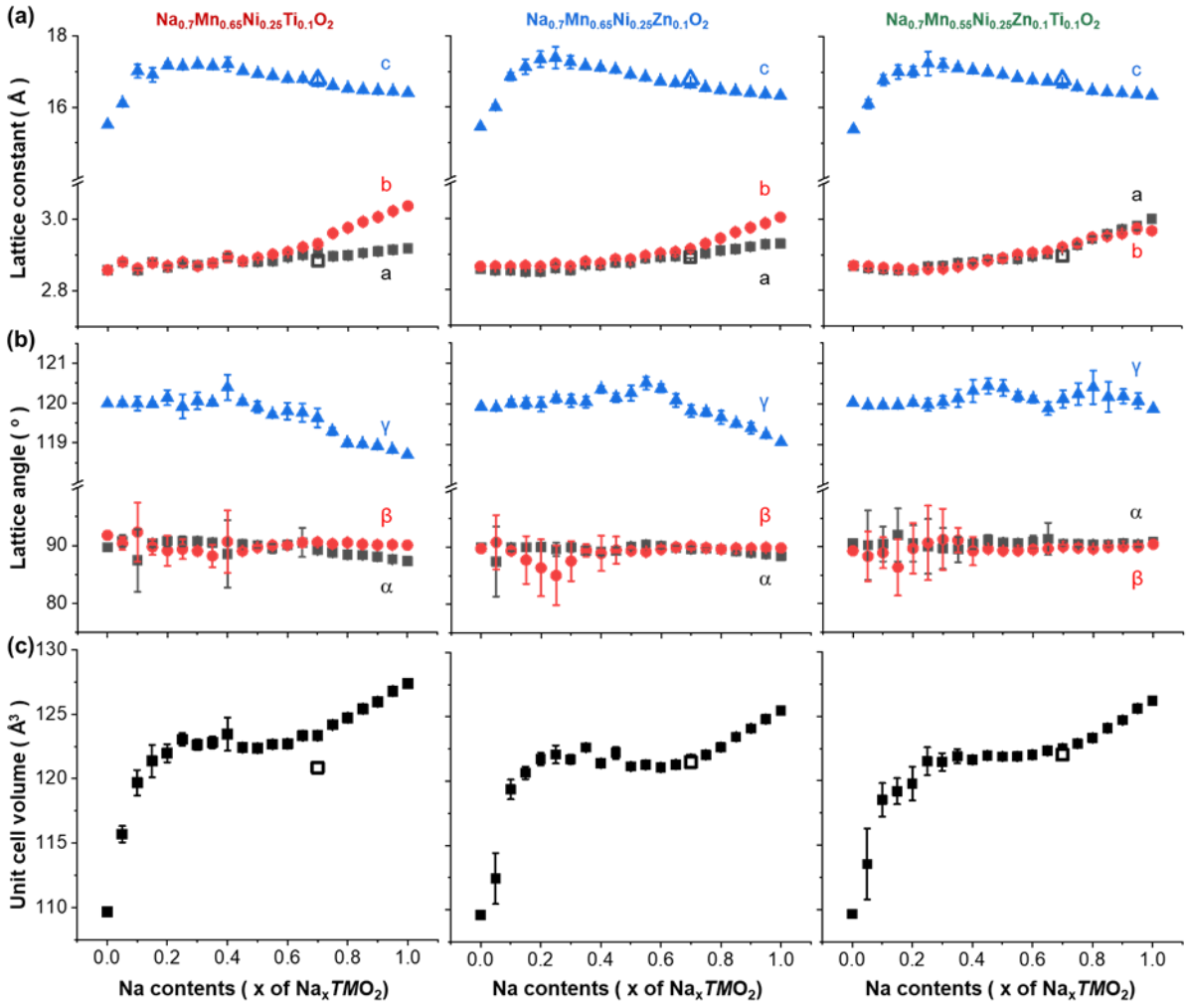

Figure S8. *Comparison of calculated lattice parameters. (a) Lattice constants, (b) lattice angles, and (c) unit cell volumes of* $Na_{0.7}Mn_{0.65}Ni_{0.25}Ti_{0.1}O_2$, $Na_{0.7}Mn_{0.65}Ni_{0.25}Zn_{0.1}O_2$ *and* $Na_{0.7}Mn_{0.58}Ni_{0.25}Zn_{0.07}Ti_{0.1}O_2$ *plotted with respect to Na compositions.*

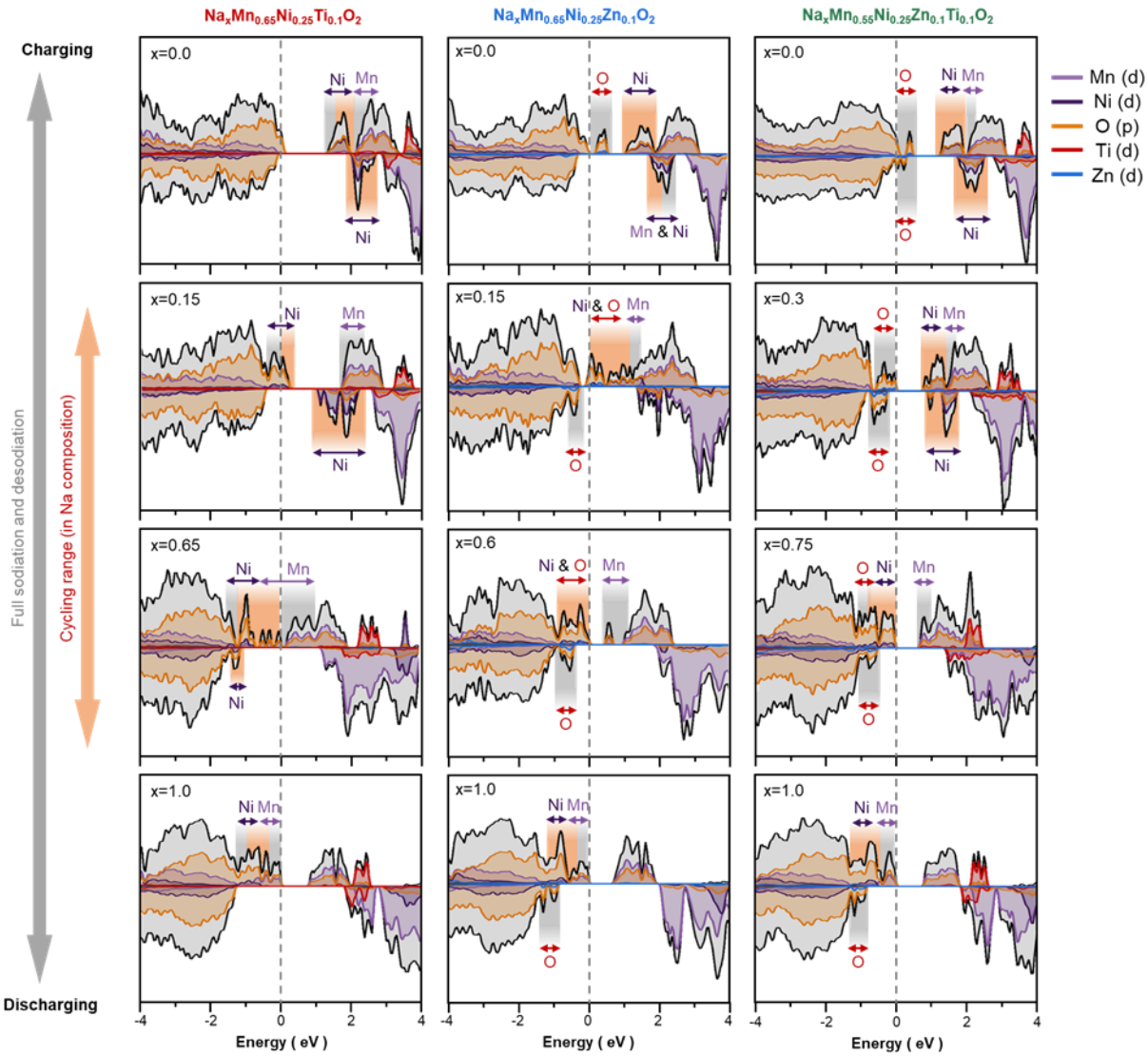

Figure S9. *Redox active elements of P3-type cathodes. Projected density of states of P3-type $Na_xMn_{0.65}Ni_{0.25}Ti_{0.1}O_2$, $Na_xMn_{0.65}Ni_{0.25}Zn_{0.1}O_2$, and $Na_xMn_{0.58}Ni_{0.25}Zn_{0.07}Ti_{0.1}O_2$ calculated for four different Na composition cases: fully desodiated case (x = 0), charged at upper voltage window limit of 4.3 V, discharged at lower voltage window limit of 2.2 V, and fully sodiated case (x = 1). Redox active electrons accessible within cycling range of 2.2-4.3 V are highlighted by orange area, whereas those only available under full sodiation/desodiation are denoted as grey area. Unlike $Na_xMn_{0.65}Ni_{0.25}Zn_{0.1}O_2$, anionic redox reaction in $Na_xMn_{0.65}Ni_{0.25}Ti_{0.1}O_2$ is difficult even after full desodiation, because of lower energy state of bonding orbitals. For $Na_xMn_{0.58}Ni_{0.25}Zn_{0.07}Ti_{0.1}O_2$, anionic redox can occur upon full desodiation, but it was rarely observed in this study because of the limited voltage window of 2.2-4.3 V (i.e., short Na composition range of $0.28 < x < 0.75$).*

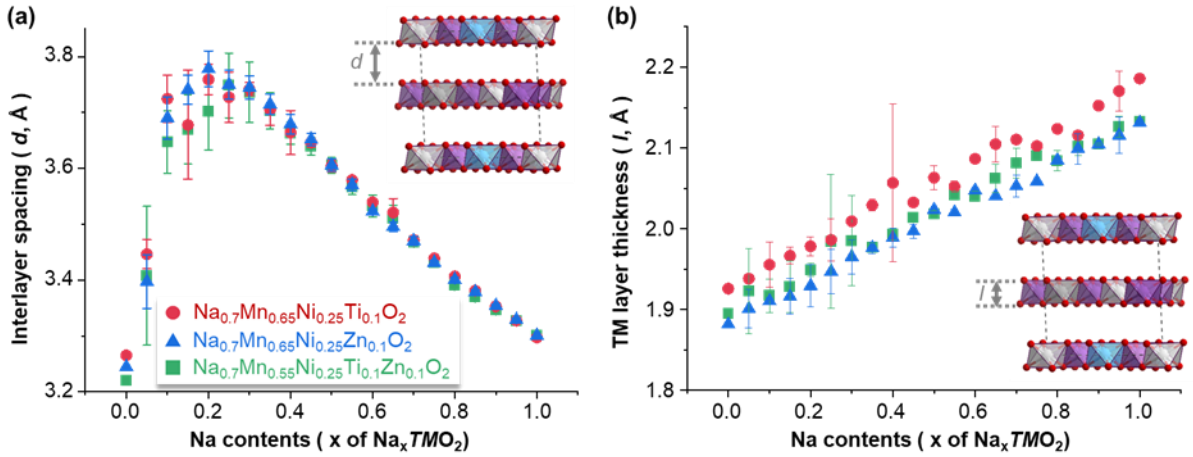

Figure S10. *Origin of the longer c-axis of Zn-substituted samples. (a) Interlayer spacings (d) and (b) TM layer thicknesses (l) of $Na_xMn_{0.65}Ni_{0.25}Zn_{0.1}O_2$, $Na_xMn_{0.65}Ni_{0.25}Ti_{0.1}O_2$ and $Na_xMn_{0.58}Ni_{0.25}Zn_{0.07}Ti_{0.1}O_2$ calculated from the optimized model structures. Mean and standard deviation of values are denoted as dots and vertical lines, respectively. Compared to Ti-substituted $Na_xMn_{0.65}Ni_{0.25}Ti_{0.1}O_2$, Zn-substituted $Na_xMn_{0.65}Ni_{0.25}Zn_{0.1}O_2$ exhibits broader interlayer spacing at low Na composition range of $0.15 \leq x \leq 0.45$. In contrary, TM thickness is the lowest for the $Na_xMn_{0.65}Ni_{0.25}Zn_{0.1}O_2$, indicating that the longer c-axis of Zn-substituted samples stems from interlayer spacing, not from the size of TM octahedra. Standard deviation values are largest for $Na_xMn_{0.58}Ni_{0.25}Zn_{0.07}Ti_{0.1}O_2$, which may arise from the complexities in the ordering of four different types of transition metal elements.*